JOURNAL OF VIROLOGY, Nov. 2010, p. 11030–11044 Vol. 84, No. 21
0022-538X/10/$12.00 doi:10.1128/JVI.02688-09


# Murine Coronavirus Receptors Are Differentially Expressed in the Central Nervous System and Play Virus Strain-Dependent Roles in Neuronal Spread[▽]

Susan J. Bender, Judith M. Phillips, Erin P. Scott,† and Susan R. Weiss*

*Department of Microbiology, University of Pennsylvania School of Medicine, Philadelphia, Pennsylvania 19104-6076*

Received 22 December 2009/Accepted 9 August 2010

**Coronavirus infection of the murine central nervous system (CNS) provides a model for studies of viral encephalitis and demyelinating disease. Mouse hepatitis virus (MHV) neurotropism varies by strain: MHV-A59 causes mild encephalomyelitis and demyelination, while the highly neurovirulent strain JHM.SD (MHV-4) causes fatal encephalitis with extensive neuronal spread of virus. In addition, while neurons are the predominant CNS cell type infected *in vivo*, the canonical receptor for MHV, the carcinoembryonic antigen family member CEACAM1a, has been demonstrated only on endothelial cells and microglia. In order to investigate whether CEACAM1a is also expressed in other cell types, *ceacam1a* mRNA expression was quantified in murine tissues and primary cells. As expected, among CNS cell types, microglia expressed the highest levels of *ceacam1a*, but lower levels were also detected in oligodendrocytes, astrocytes, and neurons. Given the low levels of neuronal expression of *ceacam1a*, primary neurons from wild-type and *ceacam1a* knockout mice were inoculated with MHV to determine the extent to which CEACAM1a-independent infection might contribute to CNS infection. While both A59 and JHM.SD infected small numbers of *ceacam1a* knockout neurons, only JHM.SD spread efficiently to adjacent cells in the absence of CEACAM1a. Quantification of mRNA for the *ceacam1a*-related genes *ceacam2* and *psg16* (*bCEA*), which encode proposed alternative MHV receptors, revealed low *ceacam2* expression in microglia and oligodendrocytes and *psg16* expression exclusively in neurons; however, only CEACAM2 mediated infection in human 293T cells. Therefore, neither CEACAM2 nor PSG16 is likely to be an MHV receptor on neurons, and the mechanism for CEACAM1a-independent neuronal spread of JHM.SD remains unknown.**

Murine coronavirus (mouse hepatitis virus [MHV]) is a member of the *Coronaviridae* family of large, enveloped RNA viruses. Central nervous system (CNS) infection with neurotropic strains of MHV provides a model for studying acute virus-induced neurological disease, with or without chronic demyelination. These neurotropic strains differ widely in terms of tropism, spread, host response, and disease outcome, making them useful for identifying viral and host determinants of neurovirulence (57). Two strains commonly used to study coronavirus-induced CNS disease are the highly neurovirulent strain JHM.SD (formerly called MHV-4) and the more neuroattenuated and hepatotropic strain A59 (4, 26). Following intracranial (i.c.) or intranasal (i.n.) inoculation, JHM.SD causes severe and uniformly lethal encephalitis, whereas A59 induces a less severe encephalomyelitis followed by chronic demyelination (57). The extreme neurovirulence of JHM.SD maps largely to the spike glycoprotein, as a recombinant A59 virus expressing the JHM.SD spike (rA59/$S_{JHM.SD}$) showed increased virulence and viral dissemination throughout the brain compared to parental A59 (41, 42). Viral genes other than the spike gene also contribute to neurovirulence (7, 23).

MHV binds to a target cell via interaction of the viral spike glycoprotein with a cellular receptor. This binding leads to a conformational change in spike that allows the virion membrane to fuse with the host cell membrane. Subsequent viral spread can occur via release of new virions from the infected cell and/or via syncytium formation mediated by viral spikes expressed on the cell surface. The receptor for MHV is the murine carcinoembryonic antigen family member CEACAM1a (also referred to as mmCGM1, BGP1a, and CD66a) (59). In the mouse, the *ceacam1* gene exists in two allelic forms, *ceacam1a* and *ceacam1b*, and the *ceacam1* alleles expressed largely determine mouse susceptibility to MHV. Mouse strains expressing *ceacam1a* (such as C57BL/6, BALB/c, and C3H) are highly susceptible, while strains homozygous for *ceacam1b* (such as SJL) are resistant to infection (10). *ceacam1a* transcripts are alternatively spliced, yielding four distinct variants in the mouse. These splice variants encode either two or four extracellular immunoglobulin-like (Ig-like) domains linked by a transmembrane domain to a short (10 amino acids) or long (73 amino acids) cytoplasmic tail (30, 31). The MHV binding site resides within the N-terminal Ig-like domain, D1 (11). This domain is present in all four isoforms of CEACAM1a, and thus all serve as functional receptors for MHV (10).

While CEACAM1a is commonly regarded as the sole *in vivo* receptor for MHV, several lines of evidence suggest the presence of an alternative receptor and/or mechanism of viral infection/spread. Curiously, despite the high predilection of neurotropic MHV strains for the CNS, CEACAM1a expression is relatively low in neural tissue compared to that in other MHV

* Corresponding author. Mailing address: Department of Microbiology, University of Pennsylvania School of Medicine, 36th Street and Hamilton Walk, Philadelphia, PA 19104-6076. Phone: (215) 898-8013. Fax: (215) 573-4858. E-mail: weisssr@mail.med.upenn.edu.

† Present address: Complete Publication Solutions, LLC, 120 Gibraltar Rd., Suite 200, Horsham, PA 19044.

▽ Published ahead of print on 25 August 2010.

targets, such as the liver and intestine (17). While CEACAM1a is highly expressed on epithelial cells, endothelial cells, and cells of hematopoietic origin (6, 17, 35), CNS expression of CEACAM1a has been demonstrated only on endothelial cells, by immunohistochemistry (16), and on microglia, by flow cytometry (44). Yet both A59 and JHM.SD infect multiple CNS cell types, with neurons being the predominant cell type infected (12, 33, 42). This apparent paradox raises the question of whether resident CNS cell types such as neurons, astrocytes, and oligodendrocytes express low levels of CEACAM1a that are simply not detected by routine methods or whether some MHV strains use an alternative mechanism to enter these cell types.

Additionally, *in vitro* studies revealed that the highly neurovirulent JHM.SD strain can spread efficiently from CEACAM1a-positive cells to cells lacking murine CEACAM1a (15, 36, 39, 55). Similar *in vitro* studies using primary mixed neural cultures demonstrated that the closely related JHM.SD cl-2 variant spreads to adjacent neural cells in the presence of CEACAM1a-blocking antibodies (34). This "receptor-independent spread" (RIS) phenomenon should more accurately be referred to as "CEACAM1a-independent spread," since the process may or may not require an alternative receptor. The generation of a knockout (KO) mouse deficient in *ceacam1a* (*ceacam1a*$^{-/-}$) further facilitated analysis of CEACAM1a-independent spread both *in vivo* and *in vitro*. Interestingly, both JHM.SD and the chimeric rA59/$S_{JHM.SD}$ strain induce lethal CNS disease in *ceacam1a*$^{-/-}$ mice, albeit at higher doses than those required for wild-type (WT) mice, while doses of A59 as high as 1 million PFU given i.c. are insufficient to cause disease (21, 33). While this finding is intriguing, it is unclear whether A59 fails to cause disease in *ceacam1a*$^{-/-}$ mice due to a lack of virus entry, a deficiency in neuronal spread in the absence of CEACAM1a, or an inability to achieve a high enough viral dose to initiate infection.

Notably, two *ceacam1a*-related genes expressed in the mouse brain encode proteins that serve inefficiently as MHV receptors when overexpressed *in vitro*. The more closely related *ceacam2* (*bgp2*) gene is uniquely expressed in the mouse and facilitates infection with both A59 and JHM.SD when transiently transfected into hamster cells (38). Additionally, the more distantly related *psg16* (*bCEA*) gene, belonging to the CEA-related pregnancy-specific glycoprotein family, was reported to function as a receptor for A59 but not JHM.SD when transfected into monkey cells (5). It is unclear how these alternative receptors compare in terms of receptor functionality, and the cellular expression patterns of these receptor genes have not been explored. Therefore, in the current study, we aimed to evaluate expression of *ceacam1a* and related genes in murine tissues and CNS cell types and to investigate the role of these receptor genes in neuronal infection and spread.

## MATERIALS AND METHODS

**Mice.** Virus-free C57BL/6 mice were purchased from the National Cancer Institute (Frederick, MD). *ceacam1a*-deficient (*ceacam1a*$^{-/-}$) mice on a C57BL/6 background were provided by Nicole Beauchemin (McGill University) (21). Mice were housed and bred at the University of Pennsylvania in accordance with Institutional Animal Care and Use Committee guidelines.

**Viruses and inoculations.** Recombinant A59 (rA59) (previously referred to as RA59, $S_{A59}$R13, or wtR13), recombinant JHM.SD (rJHM.SD) (previously referred to as RJHM and derived from the MHV-4 isolate of JHM.SD), and a chimeric recombinant expressing the JHM.SD spike in the A59 background (rA59/$S_{JHM.SD}$) (previously referred to as SJHM/RA59 or $S_4$R22) were described previously (37, 41, 42). Recombinant viruses of the same genotypes, but expressing enhanced green fluorescent protein (EGFP) in place of gene 4 (8, 27), were used to monitor infection in primary cells. Viruses were propagated in murine 17Cl1 fibroblasts and titrated by standard plaque assay on murine L2 fibroblasts. To remove cell fragments from the virus preparations, filtered virus stocks were prepared by passage through a 0.22-μm filter apparatus and were retitrated after filtration. For i.c. inoculations, 4-week-old mice were anesthetized with isoflurane, and 50 PFU of virus diluted in 30 μl phosphate-buffered saline (PBS) containing 0.75% bovine serum albumin (BSA) was injected into the left cerebral hemisphere. Mock infections were performed with lysate from 17Cl1 fibroblasts.

**Immunofluorescence.** For identification of infected cell types, brains were perfused with PBS, fixed in 10% phosphate-buffered formalin, embedded in paraffin, and sagittally sectioned. Sections were deparaffinized and rehydrated, treated with antigen-unmasking solution (Vector Labs), blocked with 1.5% normal goat serum, and dual immunolabeled with a mouse monoclonal antibody (1.16.1) directed against the MHV nucleocapsid protein (a gift from Julian Leibowitz, Texas A&M University) and a rabbit polyclonal antibody directed against either glial fibrillary acidic protein (GFAP), for astrocytes (Dako USA); Iba1, for microglia (Wako Pure Chemical Industries); OLIG2, for oligodendrocytes (Millipore); or microtubule-associated protein 2 (MAP2), for neurons (a gift from Virginia Lee, University of Pennsylvania). Primary antibodies were detected with Alexa Fluor 488- and 594-conjugated goat anti-mouse and goat anti-rabbit (Invitrogen). Cultured cells were fixed in PBS containing 4% paraformaldehyde (Electron Microscopy Sciences), blocked with 1.5% normal goat serum, and immunolabeled as described above, with the exception of microglia, which were labeled with rat monoclonal anti-CD11b (Abcam) and goat anti-rat–Alexa Fluor 594 (Invitrogen). Fluorescence was visualized with a Nikon Eclipse TE2000-U microscope, and images were acquired using Spot imaging software (Diagnostic Instruments).

**Primary hepatocyte cultures.** Primary hepatocytes were prepared from 8-week-old mice by *in situ* perfusion and digestion with liver perfusion medium (Invitrogen) and liver digestion medium (Invitrogen), respectively, followed by mechanical disruption and Percoll separation as previously described (48). Hepatocytes were seeded on BioCoat collagen I-coated plates (BD Biosciences) and were cultured overnight in RPMI 1640 medium containing 10% fetal bovine serum (FBS).

**Primary glial cultures.** Mixed glial cells were prepared from the cortices of P1-3 neonates and cultured in Dulbecco's modified Eagle's medium (DMEM) containing 10% FBS, 2 mM L-glutamine, 100 U/ml penicillin, and 100 ng/ml streptomycin for 5 to 14 days. Mixed glial cultures were enriched for either astrocytes or microglia based on differential adhesion to tissue culture plastic as previously described (1). Astrocyte cultures were routinely 90 to 95% pure, as determined by positive immunostaining for GFAP and negative staining for MAP2, CD11b, and OLIG2. Microglia cultures were routinely ≥98% pure, as determined by positive immunostaining for CD11b and negative staining for MAP2, GFAP, and OLIG2. Oligodendrocytes were prepared from forebrains of P1-3 neonates by trypsin digestion and were cultured in DMEM containing 10% FBS, 1× nonessential amino acid solution (Invitrogen), 2 mM L-glutamine, 100 U/ml penicillin, and 100 ng/ml streptomycin as previously described (13). After 24 h, culture medium was replaced with neurobasal medium containing B-27 supplement, 10 ng/ml bovine basic fibroblast growth factor (R&D Systems), 2 ng/ml recombinant human platelet-derived growth factor (R&D Systems), and 1 ng/ml recombinant human NT-3 (PeproTech Inc.). After 7 days, oligodendrocytes were removed from underlying astrocytes by gentle rinsing and were seeded onto poly-D-lysine-coated tissue culture plates. Oligodendrocyte cultures were routinely 90 to 95% pure, as determined by positive immunostaining for OLIG2 and negative immunostaining for MAP2, CD11b, and GFAP.

**Primary neuronal cultures.** Hippocampal neurons were prepared from E15-16 mouse embryos, seeded onto poly-L-lysine-coated coverslips or tissue culture plates, and cultured in neurobasal medium containing B-27 supplement (Invitrogen), 100 U/ml penicillin, 100 ng/ml streptomycin, 2 mM L-glutamine, and 4 μg/ml glutamate for 4 days in the absence of an astrocyte feeder layer, as previously described (2, 40, 43). Cortical neurons prepared from E18 mouse embryos were provided by Marc Dichter (University of Pennsylvania) (9, 50). Neuron cultures of both types were routinely 95 to 98% pure, as determined by positive immunostaining for MAP2 and negative immunostaining for CD11b, GFAP, and OLIG2. After 4 days *in vitro*, neuron cultures were inoculated with virus diluted in neurobasal medium for 1 h at 37°C, washed, and cultured for an additional 24 to 72 h in neurobasal medium. To quantify extracellular virus, neuron supernatants were collected at various times postinfection and stored at

TABLE 1. Primer sequences for qRT-PCR

| Target | Forward primer (5′–3′) | Reverse primer (5′–3′) | Product size (bp) | GenBank accession no. |
|---|---|---|---|---|
| Mouse targets | | | | |
| Beta-actin gene | CAGATGTGGATCAGCAAGCAGGA | CGCAGCTCAGTAACAGTCCGCCTA | 90 | NM_007393 |
| *ceacam1a* | | | | |
| Total | GCCTCAGCACATCTCCACAAAG | CCTCAATGGTGACTTCAGCAGTG | 109 | NM_001039185 |
| 2D | CCTGGCGCTTGGAGCCTTTG | GCTGAGTCACTGGCTGGTGT | 263 | NM_001039187 |
| 4D | GGCCTCAGTAGGACCACAGTCAAGA | CGACAAGCAGGTCAGGGTCACAG | 120 | NM_001039185 |
| S | GCATCGTGATTGGAGTTGTG | GTTGTCAGAAGGAGCCAGATCC | 99 | NM_001039187 |
| L | GGGAAGTGACCAGCGAGAT | GTGGTTGGAGGCTGAGGGTTTGT | 52 | NM_001039185 |
| *ceacam2* | CATCTCCACAAAGGGCAGGTTCC | TGTGCCAGCTAAAGGCCGAGAC | 187 | NM_007543 |
| *psg16* | GCTTCGAGGGCTTTCCTGGTACA | TGTCGGGCAATCTCAAGGTTCCTA | 63 | NM_007676, U34272 |
| MHV target | | | | |
| mRNA7 (nucleocapsid) | GGCGTCCGTACGTACCC | GGTCAGCCCAAGTGGTC | 167 | X00990 |

−80°C until titration. Fresh neurobasal medium was added to the remaining cells, and intracellular virus was released by repeated freeze-thaw cycles, with freezing to −80°C.

**Cell lines.** Murine DBT astrocytoma cells, 17Cl1 fibroblasts, and L2 fibroblasts were cultured in DMEM supplemented with 10% FBS, 10 mM HEPES, 2 mM L-glutamine, 100 U/ml penicillin, 100 ng/ml streptomycin, and 2.5 μg/ml amphotericin B. Human 293T cells were cultured in high-glucose DMEM containing 10% FBS, 100 U/ml penicillin, and 100 ng/ml streptomycin.

**Quantitative reverse transcription-PCR (qRT-PCR).** RNAs were isolated from liver, brain, and spinal cord tissues by homogenization in TRIzol reagent (Invitrogen), followed by phenol-chloroform extraction and purification with an RNeasy Mini kit (Qiagen) as previously described (49). RNAs were isolated from cultured cells by use of an RNeasy Mini kit according to the manufacturer's instructions. Tissue and cellular RNAs were DNase treated using a Turbo DNA-free kit (Ambion), and quantitative PCRs without reverse transcriptase were performed to ensure adequate removal of genomic DNA. For cDNA synthesis, 350 ng RNA was combined with 0.5 mM deoxynucleoside triphosphate (dNTP) mix (0.5 mM, total concentration; Invitrogen) and 50 ng random hexamers (Invitrogen) in a total volume of 13 μl, heated to 65°C in a PCR thermocycler for 3 min, and cooled to room temperature. Next, 1× first-strand buffer (Invitrogen), 5 mM dithiothreitol (DTT) (Invitrogen), 200 U SuperScript III reverse transcriptase (Invitrogen), and nuclease-free water were added for a final reaction volume of 20 μl, and the mixture was heated to 50°C for 60 min followed by 70°C for 15 min. cDNA was stored at −20°C until use. Quantitative PCR was performed in duplicate, using 2 μl cDNA, 12.5 μl iQ SYBR Green Supermix (Bio-Rad), and 0.4 μM (each) forward and reverse primers (listed in Table 1) in a total volume of 25 μl in an iQ5 iCycler (Bio-Rad). For copy number determination, cycle threshold ($C_T$) values were compared to a plasmid standard curve run in parallel for each target. Copy numbers are expressed as numbers of target cDNA copies per million cDNA copies of the mouse beta-actin gene (*actb*). For relative expression compared to mock-infected samples, $C_T$ values were normalized to *actb* levels, resulting in a $\Delta C_T$ value ($\Delta C_T = C_{T\ \text{target}} - C_{T\ actb}$). $\Delta\Delta C_T$ values were then calculated ($\Delta\Delta C_T = \Delta C_{T\ \text{infected}} - \Delta C_{T\ \text{mock}}$), and results are expressed as fold changes compared to mock-infected samples ($2^{-\Delta\Delta CT}$).

**Plasmids.** pLXSN-BgpC (CEACAM1a-2S) and pLXSN-BgpD (CEACAM1a-4L), used for *ceacam1a* splice variant standard curves, were provided by Nicole Beauchemin (McGill University). pCMV-SPORT6-CEACAM1, pCMV-SPORT6-CEACAM2, pCMV-SPORT6-PSG16, and pCMV-SPORT6-ACTB (mouse beta-actin partial clone) were purchased from Open Biosystems (Thermo Scientific). pCB-TVA-CEACAM1-TM, pCB-TVA-CEACAM2-TM, and pCB-TVA-PSG16-TM were made by replacing the AgeI-SacII fragment of pCB-TVA 950 (46) (obtained from Paul Bates) with PCR products containing the extracellular domains for the pCMV-SPORT6 plasmids listed above. pCB-TVA-CEACAM1-GPI, pCB-TVA-CEACAM2-GPI, and pCB-TVA-PSG16-GPI were constructed by replacing the AgeI-SacII fragment of pCB-TVA 800 (obtained from Paul Bates) as described above.

**Transfections.** To compare MHV receptor activities, human 293T cells were seeded in a 12-well plate at $1.5 \times 10^5$ cells per well and then transfected with 0.4 μg pCMV-SPORT6-CEACAM1, pCMV-SPORT6-CEACAM2, or pCMV-SPORT6-PSG16 plus 0.6 μg empty vector (1 μg total DNA), using 6 μl FuGENE 6 transfection reagent (Roche Applied Science) in serum-free DMEM. A control plasmid encoding GFP was used to assess transfection efficiency. At 36 h post-transfection, cells were inoculated with $3 \times 10^5$ PFU of virus diluted in DMEM containing 2% FBS for 1 h at 37°C. At 8 h postinfection (p.i.), cells were fixed in 4% paraformaldehyde and immunolabeled for MHV nucleocapsid protein as described above. Cell nuclei were labeled with DAPI (4′,6-diamidino-2-phenylindole), and percent infection was determined as the percentage of DAPI-positive cells per field that also stained positively for MHV nucleocapsid. To compare MHV receptor activities and surface expression levels, human 293T cells were seeded in a 24-well plate at $1.5 \times 10^5$ cells per well and then transfected with pCMV-SPORT6-CEACAM1, pCB-TVA-CEACAM1-TM, pCB-TVA-CEACAM2-TM, pCB-TVA-PSG16-TM, pCB-TVA-CEACAM1-GPI, pCB-TVA-CEACAM2-GPI, or pCB-TVA-PSG16-GPI as described above. A control plasmid encoding GFP was used to assess transfection efficiency. At 48 h post-transfection, cells were labeled with mouse M2 anti-FLAG antibody (Amersham) at 1 μg/ml, followed by goat anti-mouse–Alexa Fluor 488 at 1 μg/ml, and then fixed in 2% paraformaldehyde. Surface expression of FLAG-tagged proteins on single live cells was determined by flow cytometry (FACSCalibur flow cytometer; Becton Dickinson). In parallel, transfected cells were inoculated with $1.3 \times 10^6$ PFU of EGFP-expressing MHV strains diluted in DMEM containing 2% FBS for 1 h at 37°C. At 16 h postinfection, cells were fixed in 4% paraformaldehyde and assessed for GFP expression.

## RESULTS

**rA59 and rJHM.SD infect multiple CNS cell types *in vivo* but are largely neuronal.** To determine which CNS cell types are infected at early times after i.c. inoculation, 4-week-old C57BL/6 mice were inoculated i.c. with 50 PFU of rA59 or rJHM.SD. At days 3 and 5 p.i., infected mice were euthanized and brains were fixed for immunofluorescence. By day 3, MHV antigen was readily detected in GFAP-positive astrocytes, Iba1-positive microglia, and MAP2-positive neurons (Fig. 1A, white arrowheads), as well as in occasional OLIG2-positive oligodendrocytes (data not shown). By day 5, large patches of MHV-infected neurons were evident in both rA59- and rJHM.SD-infected brains (Fig. 1B), with only modest increases in the numbers of infected astrocytes and microglia (data not shown), consistent with previous data showing that neurons are the predominant cell type infected by these strains (12, 33, 42). Importantly, while rA59 and rJHM.SD both infect large numbers of neurons, rJHM.SD is distributed more extensively throughout the brain than rA59, which remains more focal (23).

***ceacam1a* mRNA is expressed in murine tissues, primary cells, and cell lines.** Both rA59 and rJHM.SD infect multiple cell

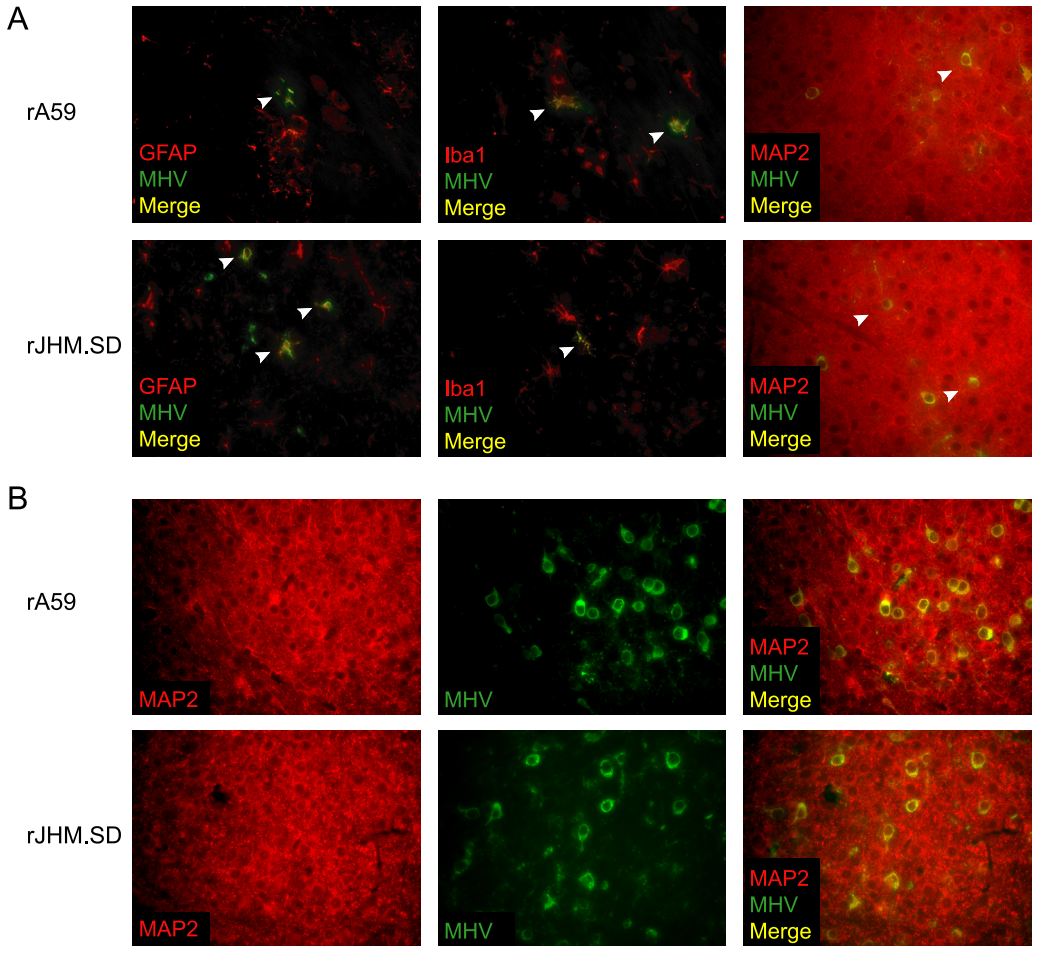


FIG. 1. MHV infection of CNS cell types. C57BL/6 mice inoculated i.c. with 50 PFU of rA59 or rJHM.SD were sacrificed at days 3 (A) and 5 (B) postinfection. Formalin-fixed, paraffin-embedded tissues were sectioned and dual immunolabeled for GFAP, Iba1, or MAP2 (red) and MHV nucleocapsid protein (green). Arrowheads indicate double-positive cells. Magnification, ×400. Data are representative of two independent experiments.

types, as described above, but microglia are the only CNS cell type previously demonstrated to express CEACAM1a protein (44). While we were able to detect CEACAM1a on microglia by flow cytometry, we were unable to demonstrate CEACAM1a protein on neurons or any glial cell types by immunoblotting, immunohistochemistry, or immunohistochemical amplification techniques such as tyramide signal amplification (PerkinElmer) (data not shown). Therefore, a qRT-PCR approach was taken to assess the expression of *ceacam1a* mRNA in murine tissues, primary CNS cells, and cell lines to determine whether susceptible CNS cells might express low levels of CEACAM1a protein not detectable by routine methods. Primers were designed to amplify a region of the N-terminal Ig-like domain. This domain contains the site of MHV spike binding and is present in all four known *ceacam1a* splice variants, thus allowing amplification of total *ceacam1a* mRNA. The results are expressed as numbers of cDNA copies of *ceacam1a* per million cDNA copies of *actb*. To determine if mRNA expression data parallel known CEACAM1a protein expression data, RNAs isolated from livers, brains, and spinal cords of 4-week-old C57BL/6 mice were subjected to qRT-PCR analysis for total *ceacam1a* mRNA, using the primer set listed in Table 1. Consistent with published data showing that the liver expresses more CEACAM1a protein than the brain (17, 59), *ceacam1a* mRNA levels in the liver were approximately 10- to 100-fold higher than those in both the brain and spinal cord in WT mice (Fig. 2A). To ensure the specificity of these primers, qRT-PCR analysis was performed on tissue RNA from *ceacam1a*$^{-/-}$ (KO) mice. As expected, no product was amplified from *ceacam1a*$^{-/-}$ RNA (Fig. 2A), confirming the specificity of the assay.

To evaluate which CNS cell types express *ceacam1a*, enriched primary cell cultures were generated from WT mice as described in Materials and Methods. RNAs isolated from these cell cultures were then subjected to qRT-PCR analysis of total *ceacam1a* expression. Primary hepatocytes and microglia, two cell types known to express CEACAM1a protein (17, 44), were used as positive controls. As expected, both hepatocytes and microglia were positive for *ceacam1a* expression, with hepatocytes expressing approximately 10-fold higher levels than microglia (Fig. 2B). Interestingly, *ceacam1a* expression was readily detected in both astrocyte and oligodendrocyte cultures, albeit at lower levels than in microglia (Fig. 2B). While *ceacam1a* expression was also detected in cortical and

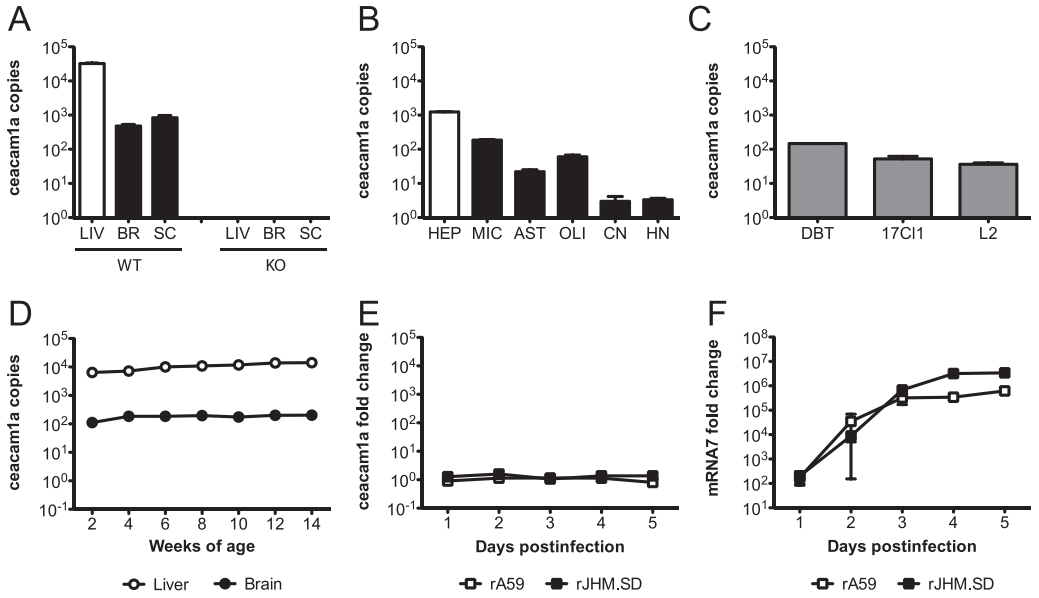


FIG. 2. *ceacam1a* mRNA expression in murine tissues, primary cells, and cell lines. RNAs isolated from 4-week-old C57BL/6 mouse tissues (A), primary cell cultures (B), cell lines (C), 2- to 14-week-old C57BL/6 mouse tissues (D), and C57BL/6 mouse brains (E and F) from mice inoculated i.c. with 50 PFU of rA59 or rJHM.SD were analyzed by qRT-PCR for expression of total *ceacam1a* mRNA (A to E) or mRNA7 (F). Results are expressed as numbers of cDNA copies of *ceacam1a* per million cDNA copies of *actb* (A to D) or as fold changes compared to mock-infected controls (E and F). Error bars represent standard errors of the means ($n = 3$). Data are representative of two or more independent experiments. LIV, liver; BR, brain; SC, spinal cord; WT, wild type; KO, *ceacam1a*$^{-/-}$; HEP, hepatocyte; MIC, microglia; AST, astrocyte; OLI, oligodendrocyte; CN, cortical neuron; HN, hippocampal neuron.

hippocampal neuron cultures, these expression levels were extremely low (Fig. 2B). Importantly, since primary cell cultures are enriched but not entirely pure, immunofluorescence labeling was performed as described in Materials and Methods to identify contaminating cell types in the individual cultures. Microglia cultures were routinely ≥98% pure, with rare astrocyte and oligodendrocyte contamination (data not shown). Astrocyte cultures were routinely 90 to 95% pure, with contaminating microglia and rare oligodendrocytes (data not shown). Oligodendrocyte cultures were routinely 90 to 95% pure, with contaminating astrocytes and rare microglia (data not shown). Neuron cultures were routinely 95 to 98% pure, with contaminating astrocytes, oligodendrocytes, and rare microglia (data not shown). It is important to consider these low levels of contaminating cells in interpreting the qRT-PCR results obtained for primary cell cultures.

Murine DBT, 17Cl1, and L2 cell lines are routinely used for propagation and/or titration of MHV. DBT cells are derived from astrocytoma tissues in CDF1 mice (22), whereas 17Cl1 and L2 fibroblasts are derived from the BALB/c 3T3 cell line and the C3H/An L929 cell line, respectively (52). Given the different mouse strains of origin as well as ongoing propagation in tissue culture, it was important to characterize the levels of *ceacam1a* expression in these cell lines. To this end, RNAs isolated from DBT, 17Cl1, and L2 cells were subjected to qRT-PCR analysis of total *ceacam1a* expression. As expected, *ceacam1a* mRNA was readily detected in all three cell lines (Fig. 2C), consistent with their permissiveness to MHV infection *in vitro*. Furthermore, all cell lines examined showed similar levels of *ceacam1a* expression (Fig. 2C).

WT mice exhibit age-dependent differences in susceptibility to CNS infection with some neurotropic strains of MHV, including rA59. Since *ceacam1a* expression is developmentally regulated in mouse embryos (20), it was of interest to determine if *ceacam1a* mRNA levels in the CNS changed with age in postnatal mice. To this end, RNAs were isolated from liver and brain tissues of WT mice aged 2 to 14 weeks. This age range encompasses the different subsets of weanling and adult mice typically used for MHV studies. Interestingly, *ceacam1a* expression levels were relatively stable in both the liver and brain at all ages observed (Fig. 2D), suggesting that age-related differences in MHV susceptibility are not due to CEACAM1a expression.

Previous flow cytometric studies demonstrated that CEACAM1a expression is downregulated on microglia during acute infection of BALB/c mice with the J.2.2v-1 variant of JHM.SD; this downregulation, largely mediated by CD4 T cells, is restored following viral control (44). To determine if MHV infection affected *ceacam1a* expression in the whole brain (including brain-resident cells not easily observed by flow cytometry), C57BL/6 mice were inoculated i.c. with 50 PFU of rA59 or rJHM.SD, and RNAs were isolated on days 1 to 5 postinfection. This period was chosen to precede the CD4 T-cell peak in the brain (23) in order to examine whether acute infection and/or early host responses also affected *ceacam1a* expression. Within this period of acute infection, *ceacam1a* expression levels were unchanged compared to those in mock-infected brains (Fig. 2E). Importantly, these *ceacam1a* expression levels remained constant despite robust levels of virus replication, as demonstrated by qRT-PCR analysis of nucleocapsid mRNA (mRNA7) (Fig. 2F). Therefore, early host responses do not affect *ceacam1a* expression.

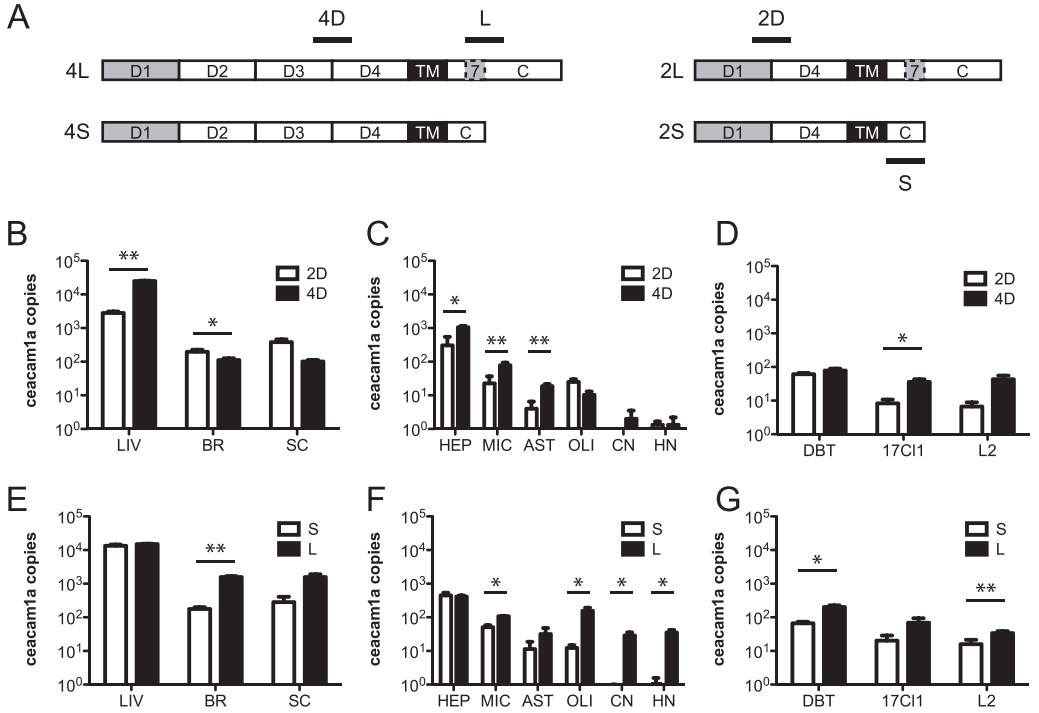


FIG. 3. *ceacam1a* splice variant expression in murine tissues, primary cells, and cell lines. (A) Schematic representing *ceacam1a* splice variants. (B to G) RNAs isolated from 4-week-old C57BL/6 mouse tissues (B and E), primary cell cultures (C and F), and cell lines (D and G) were analyzed by qRT-PCR for *ceacam1a* expression of 2 versus 4 Ig-like domains (B to D) or short versus long cytoplasmic tails (E to G). Results are expressed as numbers of cDNA copies of *ceacam1a* per million cDNA copies of *actb*. Error bars represent standard errors of the means ($n = 3$). *, $P \leq 0.05$; **, $P \leq 0.005$ (determined by paired *t* tests). Data are representative of two independent experiments. 2D, two extracellular Ig-like domains; 4D, four extracellular Ig-like domains; S, short cytoplasmic tail due to exclusion of exon 7; L, long cytoplasmic tail due to inclusion of exon 7.

***ceacam1a* splice variant mRNAs are differentially expressed in murine tissues and primary cells.** The CEACAM1a proteins containing two Ig-like domains (2D) have been suggested to be less efficient receptors than those expressing all four domains (4D) (3), which has the potential to affect MHV tropism; for example, if neurons were to express predominantly 2D isoforms, one might hypothesize that neurotropic strains are better able to use 2D isoforms than are nonneurotropic strains. In addition, the CEACAM1a isoforms with short cytoplasmic tails (S) lack some of the signaling functions of the long-tailed (L) isoforms (18, 25), which could affect infection outcomes. To more fully characterize the expression patterns of *ceacam1a* in CNS tissues and cell types, primer sets were designed to detect 2D versus 4D *ceacam1a* splice variants and short versus long cytoplasmic tails (S versus L). Primer sets are listed in Table 1, and a schematic depicting primer amplification sites is shown in Fig. 3A. While traditional RT-PCR can be used to distinguish all four splice variants based on product size alone, such assays are complicated by differences in amplification efficiency for shorter versus longer splice variants. While the qRT-PCR assay described here does not allow for distinction of each individual splice variant (2S, 2L, 4S, and 4L), it does allow for more careful quantification of 2D versus 4D species and S versus L species. As shown in Fig. 3A, 2D primers amplify a region at the splice junction between D1 and D4, whereas 4D primers amplify a region at the junction of D3 and D4. Similarly, S primers amplify the region where exon 7 has been removed by splicing, whereas L primers encompass a portion of exon 7 (Fig. 3A). Plasmids carrying *ceacam1a-2S* (BgpC) and *ceacam1a-4L* (BgpD) were used to construct standard curves for copy number determination by qRT-PCR.

Using these primer sets, the tissue and cellular RNAs described for Fig. 2 were analyzed by qRT-PCR to compare splice variant expression. As shown in Fig. 3B, 4D variants were expressed at significantly higher levels than those of 2D variants in the liver, whereas 2D variants were expressed more highly in the brain (2D variants also predominated in the spinal cord, but the difference was not statistically significant). Interestingly, while primary hepatocytes mimicked the expression (4D > 2D) observed in the liver, most primary CNS cell types also expressed 4D variants at higher levels than those of the 2D variants (Fig. 3C). This difference in brain expression versus primary cells may reflect the contribution of an additional cell type *in vivo*, such as endothelial cells, that was not analyzed in the primary cell panel. A notable exception in the primary cell panel was the oligodendrocyte cultures, which expressed slightly more 2D than 4D species, though the difference was not statistically significant (Fig. 3C). The absence of the 4D > 2D pattern seen in other primary cell types suggests that oligodendrocytes themselves express *ceacam1a* and that the total *ceacam1a* expression level shown in Fig. 2B is not due entirely to contaminating microglia or astrocytes. Cell line expression of *ceacam1a* isoforms also differed slightly, with DBT cells expressing relatively equal levels of 2D and 4D variants, while 17Cl1 fibroblasts expressed higher levels of 4D species than 2D species; L2 fibroblasts also expressed predominantly 2D spe-

cies, but the difference was not statistically significant (Fig. 3D). The pattern of 2D versus 4D splice variants did not suggest any significance for MHV tropism.

Since the length of the cytoplasmic tail may affect infection outcome, tissue and cellular RNAs were analyzed for expression of *ceacam1a* mRNA species encoding S versus L cytoplasmic tails. Interestingly, the liver exhibited relatively even expression of S and L variants, while L variants predominated over S variants in the brain (L variants also predominated in the spinal cord, but the difference was not statistically significant) (Fig. 3E). In terms of S versus L tails, the primary cells analyzed mimicked the expression seen in the tissues from which they were derived (Fig. 3F). Expression in all three cell lines showed a similar pattern as well, with L species predominating slightly over S species in DBT cells and L2 fibroblasts (L species appeared more highly expressed in 17Cl1 fibroblasts as well, but the difference was not statistically significant) (Fig. 3G). Again, we did not detect any expression pattern which would explain differences in MHV tropism.

**rJHM.SD spreads in wild-type neuron cultures despite low levels of infectious virus.** To determine whether the low levels of *ceacam1a* message detected in enriched primary neuron cultures were significant for MHV infection, we infected neurons from wild-type and *ceacam1a*$^{-/-}$ mice with rA59 and rJHM.SD and assayed for virus entry and spread. Hippocampal neuron cultures were generated from embryonic C57BL/6 mice and inoculated with 1 PFU/cell of filtered rA59, rJHM.SD, or chimeric recombinant A59 virus expressing the JHM.SD spike (rA59/$S_{JHM.SD}$); virus stocks were filtered prior to neuronal inoculations to remove residual cell debris. Recombinant versions of these viruses expressing EGFP were used in parallel to monitor infection over time and revealed widespread infection with all virus strains by 72 h postinfection (data not shown). Therefore, cells were fixed at 72 h postinfection and immunolabeled for MAP2 and the MHV nucleocapsid protein as described in Materials and Methods. As expected, all three viruses were able to infect and spread in wild-type cultured neurons, as evidenced by colocalization of MAP2 and MHV antigen (Fig. 4A); however, foci of rJHM.SD- and rA59/$S_{JHM.SD}$-infected neurons were typically larger than rA59-infected foci, consistent with previous results (42). To investigate whether spread in neuron cultures was occurring between adjacent cells or via virus release, cell lysates and culture supernatants were collected at 24, 48, and 72 h postinfection, and infectious virus was titrated by standard plaque assay on L2 cell monolayers. Interestingly, while rA59 replicated to relatively high titers within cells, rJHM.SD and rA59/$S_{JHM.SD}$ titers in cell lysates were approximately 10- to 100-fold lower than rA59 titers at all three time points (Fig. 4B). Virus release from infected neuron cultures paralleled the intracellular differences, with extracellular rA59 titers exceeding rJHM.SD titers by up to 1,000-fold by 72 h postinfection (Fig. 4C). Thus, both rJHM.SD and rA59/$S_{JHM.SD}$ spread well in wild-type neurons, despite relatively low levels of virus replication and release, suggesting that spread between adjacent cells is likely to be the major route of rJHM.SD dissemination in neurons.

**rJHM.SD spreads extensively in *ceacam1a*$^{-/-}$ neurons.** To determine if MHV entry and spread in neurons are dependent on the CEACAM1a receptor, hippocampal neurons were generated from embryonic *ceacam1a*$^{-/-}$ mice and inoculated with 1 PFU/cell of filtered rA59, rJHM.SD, or chimeric rA59/$S_{JHM.SD}$. Recombinant versions of these viruses expressing EGFP were again used in parallel to monitor the spread of infection (data not shown). Cells were fixed at 72 h postinfection and immunolabeled for MAP2 and MHV nucleocapsid protein as described for Fig. 4. Surprisingly, all three viruses were able to infect *ceacam1a*$^{-/-}$ neurons, as evidenced by colocalization of MAP2 and MHV antigen (Fig. 5). However, foci of infection were much more rare (typically 1 to 3 infected foci per coverslip) for all virus strains in *ceacam1a*$^{-/-}$ neuron cultures than the numerous coalescing foci of infection observed in wild-type neuron cultures (data not shown). Thus, virus infection of neuron cultures was much less efficient in the absence of CEACAM1a. Strikingly, though all viruses were able to enter individual cells in the *ceacam1a*$^{-/-}$ neuron cultures, only rJHM.SD and rA59/$S_{JHM.SD}$ spread efficiently to adjacent cells (Fig. 5). By 72 h postinfection, rA59 remained localized to one or two *ceacam1a*$^{-/-}$ neurons, while viruses expressing the JHM.SD spike spread similarly in *ceacam1a*$^{-/-}$ and wild-type cultures (Fig. 4A and 5). Similar differences in spread were observed in blocking experiments in which wild-type neurons were infected with rA59 or rJHM.SD and then treated with CEACAM1a-blocking antibody to evaluate neuronal spread in the absence of CEACAM1a (data not shown). Thus, while MHV entry into neural cells appears largely dependent on *ceacam1a* expression, only rA59 appears to require *ceacam1a* expression for efficient spread among adjacent neurons. This finding is consistent with previous studies showing that *ceacam1a*$^{-/-}$ mice are susceptible to infection with viruses expressing the JHM.SD spike but resistant to rA59 (33). Taken together, these results imply that the low levels of *ceacam1a* detected in enriched primary neuron cultures are significant for infection by A59 but not for infection by JHM.SD.

***ceacam2* mRNA is expressed at low levels in the murine liver and CNS.** To determine if an alternative CEACAM1a-related receptor might be positioned to mediate viral infection/spread in *ceacam1a*$^{-/-}$ mice and neuron cultures, primers were designed to amplify the N-terminal Ig-like or equivalent domain of *ceacam2* and *psg16* (*bCEA*), two *ceacam1a*-related genes that encode proteins that serve inefficiently as MHV receptors when overexpressed *in vitro* (5, 38). Primer sequences are shown in Table 1. Using the tissue and cellular RNAs described for Fig. 2, qRT-PCR was performed to detect expression of *ceacam2*, the most closely related gene to *ceacam1a* in the mouse. Results are expressed as numbers of cDNA copies of *ceacam2* per million cDNA copies of *actb*. As shown in Fig. 6A, *ceacam2* mRNA was expressed at similarly low levels in both liver and CNS tissues of WT mice. Notably, CNS expression of *ceacam2* was relatively unchanged in the absence of *ceacam1a* (KO), while liver expression was slightly increased compared to that in WT mice (Fig. 6A); however, only one set of KO tissues ($n = 3$) was available for qRT-PCR analysis. Interestingly, despite detectable levels of *ceacam2* mRNA in both liver and CNS tissues, low to no expression of *ceacam2* was observed in the primary cell types studied, with only microglia and oligodendrocyte cultures showing consistent low-level expression (Fig. 6B). Thus, other resident cell types, such as endothelial cells, likely contribute to the *ceacam2* expression observed in the liver and CNS. Interestingly, when cell lines

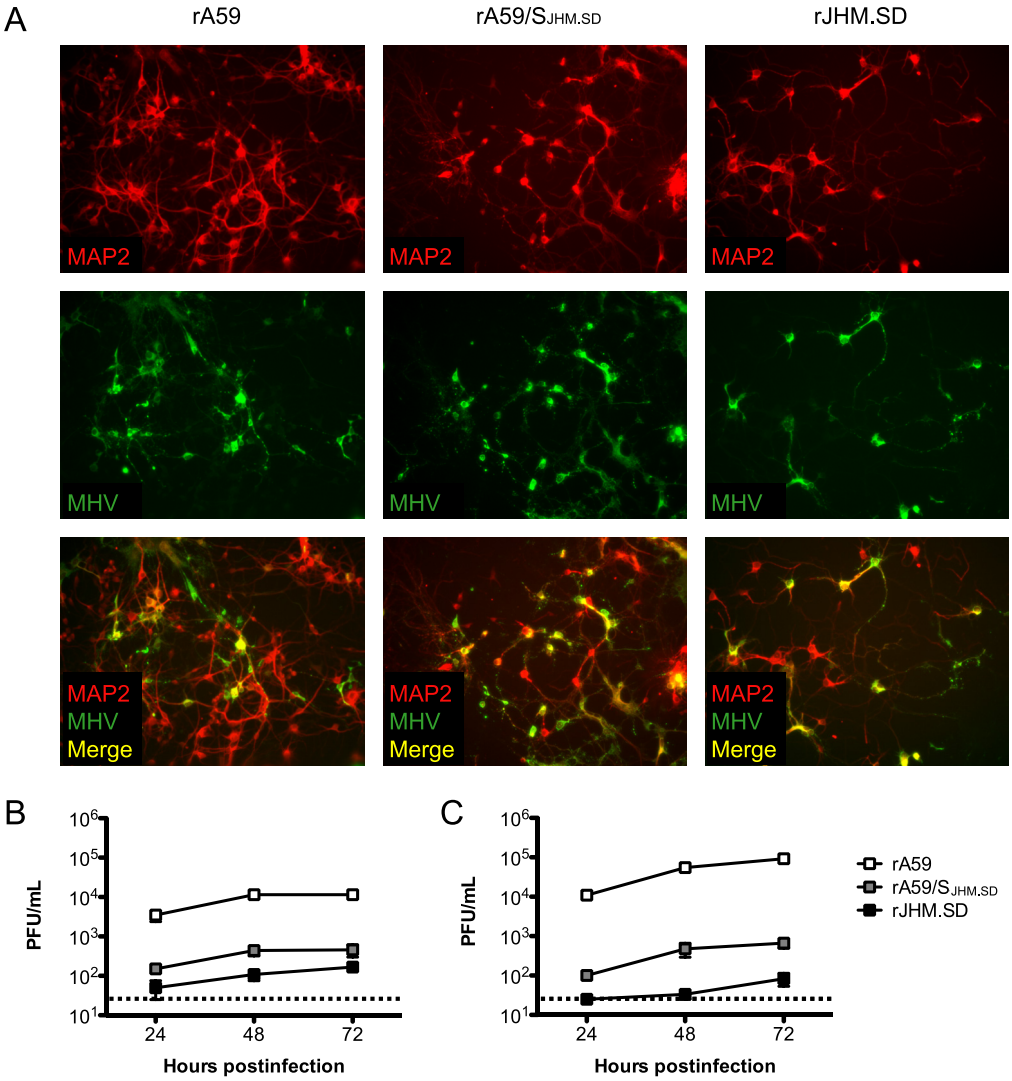


FIG. 4. MHV infection and replication in wild-type neuron cultures. Hippocampal neurons generated from C57BL/6 mice were inoculated with 1 PFU/cell of rA59, rA59/$S_{JHM.SD}$, or rJHM.SD. (A) Cells were fixed at 72 h postinfection and dual immunolabeled for MHV nucleocapsid protein (green) and MAP2 (red). Magnification, ×200. Cell lysates (B) and culture supernatants (C) were collected at 24, 48, and 72 h postinfection, and infectious virus was titrated by standard plaque assay on L2 cell monolayers. Error bars represent standard errors of the means ($n = 3$); the dotted line indicates the limit of detection. Data are representative of two or more independent experiments.

were observed, *ceacam2* expression was detectable in L2 and, to a lesser extent, DBT cells but not in 17Cl1 cells (Fig. 6C). As with *ceacam1a*, *ceacam2* expression stayed relatively constant in mice from 2 to 14 weeks of age (Fig. 6D) and was not markedly affected by MHV infection (Fig. 6E).

**PSG16 (bCEA) mRNA is expressed in the murine CNS and primary neurons.** Using the tissue and cellular RNAs described for Fig. 2, qRT-PCR was performed to detect expression of *psg16* (*bCEA*), a gene more distantly related to *ceacam1a* and described solely for the murine CNS (5). The results are expressed as numbers of cDNA copies of *psg16* per million cDNA copies of *actb*. Consistent with the previously published data (5), *psg16* expression was readily detected in the brains and spinal cords of both WT and KO mice, while expression was negligible in the liver (Fig. 7A). Interestingly, when RNAs from primary cells were examined, *psg16* expression was detected exclusively in neurons (Fig. 7B). As expected given the data in Fig. 7B, DBT, 17Cl1, and L2 cells were all negative for *psg16* expression (Fig. 7C). As with *ceacam1a* and *ceacam2*, *psg16* expression remained constant in the murine CNS in mice from 2 to 14 weeks of age (Fig. 7D) and was not significantly affected by MHV infection (Fig. 7E). The neuronal localization of *psg16* expression suggested that PSG16 might substitute for CEACAM1a to facilitate MHV entry or spread in neurons. Therefore, the functionality of this receptor was investigated.

**CEACAM2 mediates MHV entry in human 293T cells.** While CEACAM2 and PSG16 are both known to mediate inefficient MHV infection when overexpressed *in vitro* (5, 38), their functionality as MHV receptors has not been compared directly. Furthermore, PSG16 reportedly serves as a receptor for A59 but not JHM.SD (5). To evaluate receptor activity,

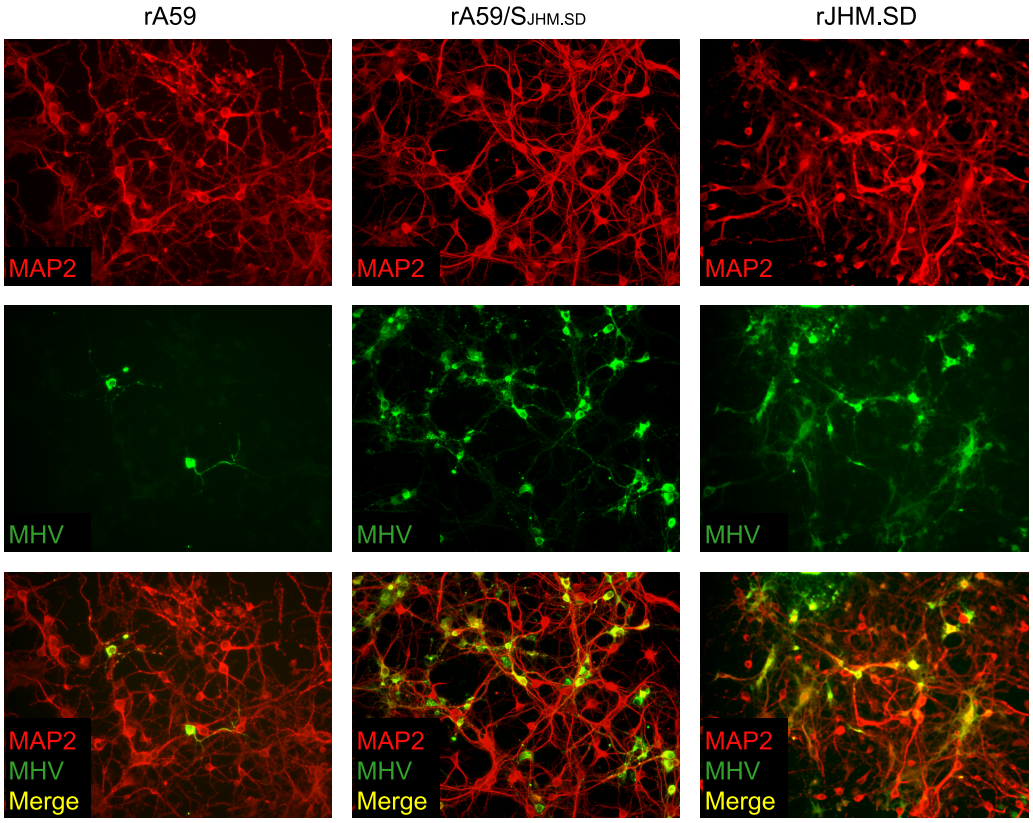


FIG. 5. MHV infection in *ceacam1a*$^{-/-}$ neuron cultures. Hippocampal neurons generated from *ceacam1a*$^{-/-}$ mice were inoculated with 1 PFU/cell of rA59, rA59/$S_{JHM.SD}$, or rJHM.SD. Cells were fixed at 72 h postinfection and dual immunolabeled for MHV nucleocapsid protein (green) and MAP2 (red). Magnification, ×200. Data are representative of two or more independent experiments.

human 293T cells were transfected with equal amounts of plasmid DNA encoding CEACAM1a, CEACAM2, or PSG16, using FuGENE 6 transfection reagent as described in Materials and Methods. The *psg16* mRNA has been isolated twice, from the mouse brain (bCEA) (5) and from a retinal cDNA library (51); the C terminus of bCEA is similar to those of other murine PSG family members, while the retinal isoform has an additional splice site resulting in an altered C terminus. Since the bCEA clone is no longer available, the retinal isoform was used. At 36 h posttransfection, cells were inoculated with 1 PFU/cell of rA59 or rJHM.SD and fixed at 8 h postinfection for immunofluorescence detection of MHV antigen; this time point was selected to allow approximately one round of MHV infection. Parallel transfection with a plasmid encoding GFP was performed to assess transfection efficiency (Fig. 8C). Quantification of MHV infection is shown in Fig. 8B. As expected, CEACAM1a mediated robust infection with both rA59 and rJHM.SD, whereas CEACAM2 was much less efficient at mediating entry (Fig. 8A and B). Importantly, no MHV antigen staining was observed in mock-infected cells or cells transfected with vector alone (Fig. 8A). Furthermore, transfection of larger amounts of receptor cDNA did not increase infection rates but did, particularly in the case of CEACAM1a, cause cells to cluster together (data not shown). Interestingly, PSG16 did not mediate infection with either rA59 or rJHM.SD in this assay (Fig. 8A), suggesting inefficient expression levels or a complete lack of cell surface expression and/or receptor functionality.

All known murine PSG proteins, with the possible exception of PSG16, are secreted rather than localized to the cell surface; in addition, relative to other murine PSG family members, both isoforms of PSG16 are missing part of the first V-type Ig domain, including the signal sequence, which appears to be completely absent in PSG16. Despite previous results (5), it seems unlikely that either form of PSG16 reaches the cell surface, and the published antibody is unavailable for verification. However, it is possible that PSG16 is available to MHV on the surfaces of neurons due to some cell type-specific transport mechanism. To determine whether PSG16 can act as an MHV receptor when targeted specifically to the cell surface, we generated chimeric constructs incorporating the extracellular Ig-like domains of PSG16 with the signal sequence and membrane anchor domains of the avian retrovirus receptor TVA, which has been used successfully in the past to create chimeric virus receptors (47). Analogous CEACAM1a and CEACAM2 constructs with the TVA signal sequence and membrane anchor domain were constructed as positive controls as well as to normalize expression levels. TVA is expressed as transmembrane and glycosylphosphatidylinositol (GPI)-anchored isoforms; PSG and both CEACAM proteins were expressed with both types of membrane anchors, for a total of six chimeras. A single FLAG epitope tag was included

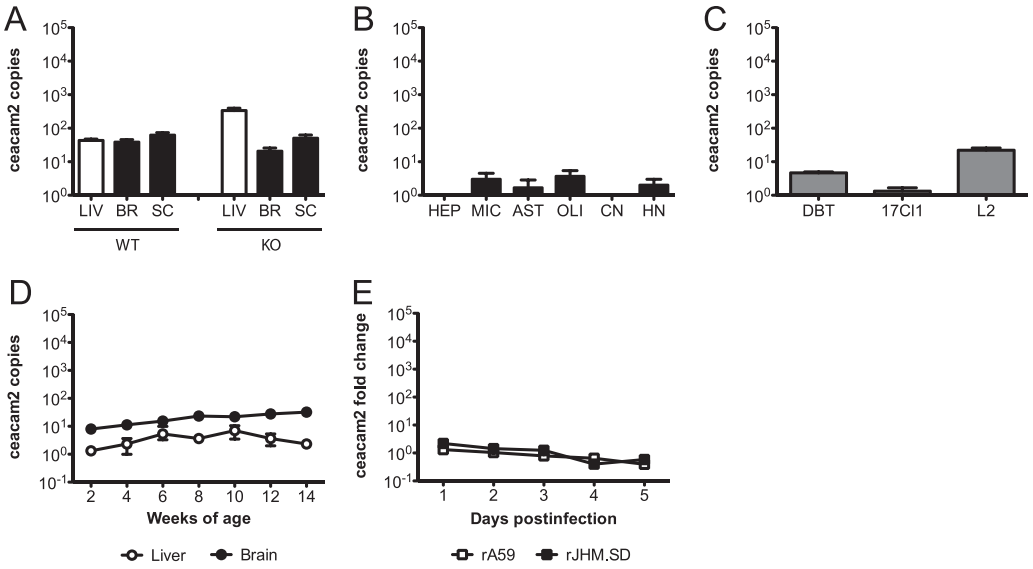


FIG. 6. *ceacam2* mRNA expression in murine tissues, primary cells, and cell lines. RNAs isolated from 4-week-old C57BL/6 mouse tissues (A), primary cell cultures (B), cell lines (C), 2- to 14-week-old C57BL/6 mouse tissues (D), and C57BL/6 mouse brains from mice inoculated i.c. with 50 PFU of rA59 or rJHM.SD (E) were analyzed by qRT-PCR for expression of *ceacam2* mRNA. Results are expressed as numbers of cDNA copies of *ceacam2* per million cDNA copies of *actb* (A to D) or as fold changes compared to mock-infected controls (E). Error bars represent standard errors of the means ($n = 3$). Data are representative of two or more independent experiments.

at the extracellular domain-membrane anchor junction of each chimera to provide uniform antibody detection. 293T cells were transfected with the TVA-CEA chimeras, and at 48 h posttransfection, surface expression was measured by flow cytometry, all as described in Materials and Methods. The transfected cells were infected with rA59 or rA59/$S_{JHM.SD}$ expressing EGFP; since the chimeric receptors were less efficient than wild-type CEACAM1a, 5 PFU/cell was used. Cells were fixed at 16 h postinfection to allow full expression of EGFP (8). Both transmembrane and GPI-anchored forms of CEACAM1a supported MHV entry, albeit less efficiently than wild-type CEACAM1a (Fig. 9), confirming that only the Ig-like domains of CEACAM1a are required for receptor activity. Like the parent proteins, the CEACAM2 chimeras were less efficient than the CEACAM1a analogs; however, the surface expression of the CEACAM2 constructs was consistently lower than that of the CEACAM1a constructs, which may account in part for the differences in

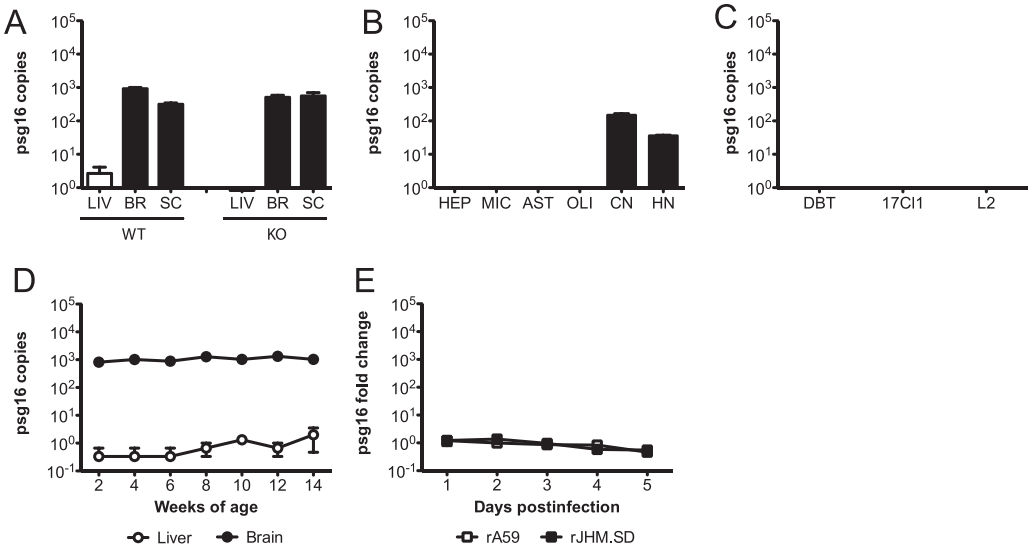


FIG. 7. *psg16* (*bCEA*) mRNA expression in murine tissues, primary cells, and cell lines. RNAs isolated from 4-week-old C57BL/6 mouse tissues (A), primary cell cultures (B), cell lines (C), 2- to 14-week-old C57BL/6 mouse tissues (D), and C57BL/6 mouse brains from mice inoculated i.c. with 50 PFU rA59 or rJHM.SD (E) were analyzed by qRT-PCR for expression of *psg16* mRNA. Results are expressed as numbers of cDNA copies of *psg16* per million cDNA copies of *actb* (A to D) or as fold changes compared to mock-infected controls (E). Error bars represent standard errors of the means ($n = 3$). Data are representative of two or more independent experiments.

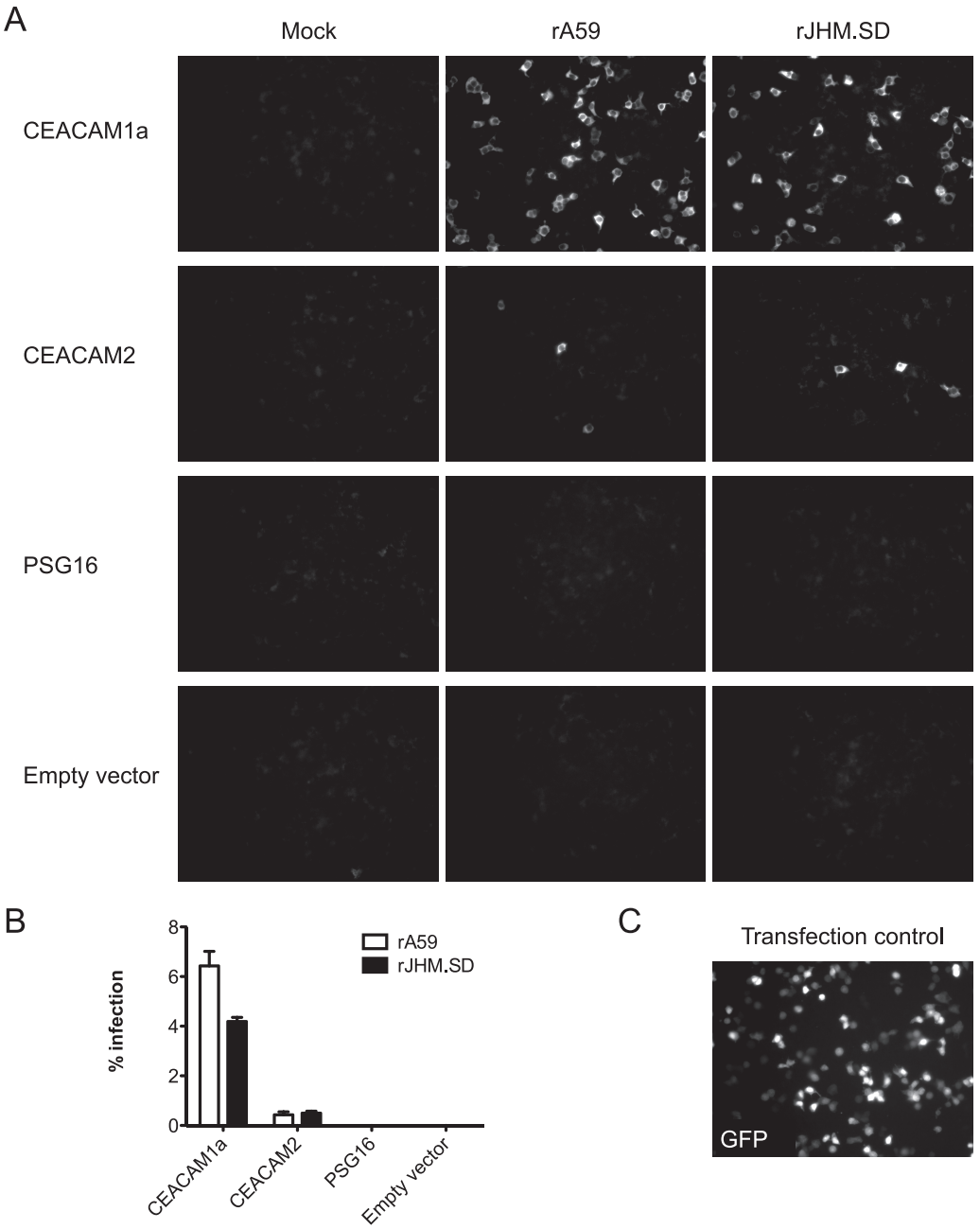


FIG. 8. MHV infection of 293T cells transfected with receptor. Human 293T cells were transfected with expression plasmids encoding CEACAM1a, CEACAM2, or PSG16 or with empty vector by use of FuGENE 6 transfection reagent. (A) Cells were infected at 36 h posttransfection with approximately 1 PFU/cell of rA59 or rJHM.SD or mock infected, fixed at 8 h postinfection, and immunolabeled for MHV nucleocapsid protein. (B) Quantification of infected cells. Error bars represent standard errors of the means ($n = 3$). (C) GFP transfection control showing transfection efficiency. Magnification, ×200. Data are representative of two or more independent experiments.

receptor activity. The PSG16 constructs failed to support MHV entry or to measurably reach the cell surface, suggesting that the Ig-like domains either misfold or are specifically targeted away from the cell surface in this system. While the extracellular Ig-like domains of both CEACAM1a and CEACAM2 are sufficient for MHV infection, we were not able to assess the MHV receptor activity of the extracellular domains of PSG16.

## DISCUSSION

Some strains of MHV are strongly neurotropic despite remarkably low expression levels of CEACAM1a, the canonical entry receptor, in the murine CNS; other MHV targets, such as the liver, express much higher levels of CEACAM1a (17, 59). At the cellular level, astrocytes, oligodendroglias, and especially neurons are infected during CNS disease (Fig. 1), despite

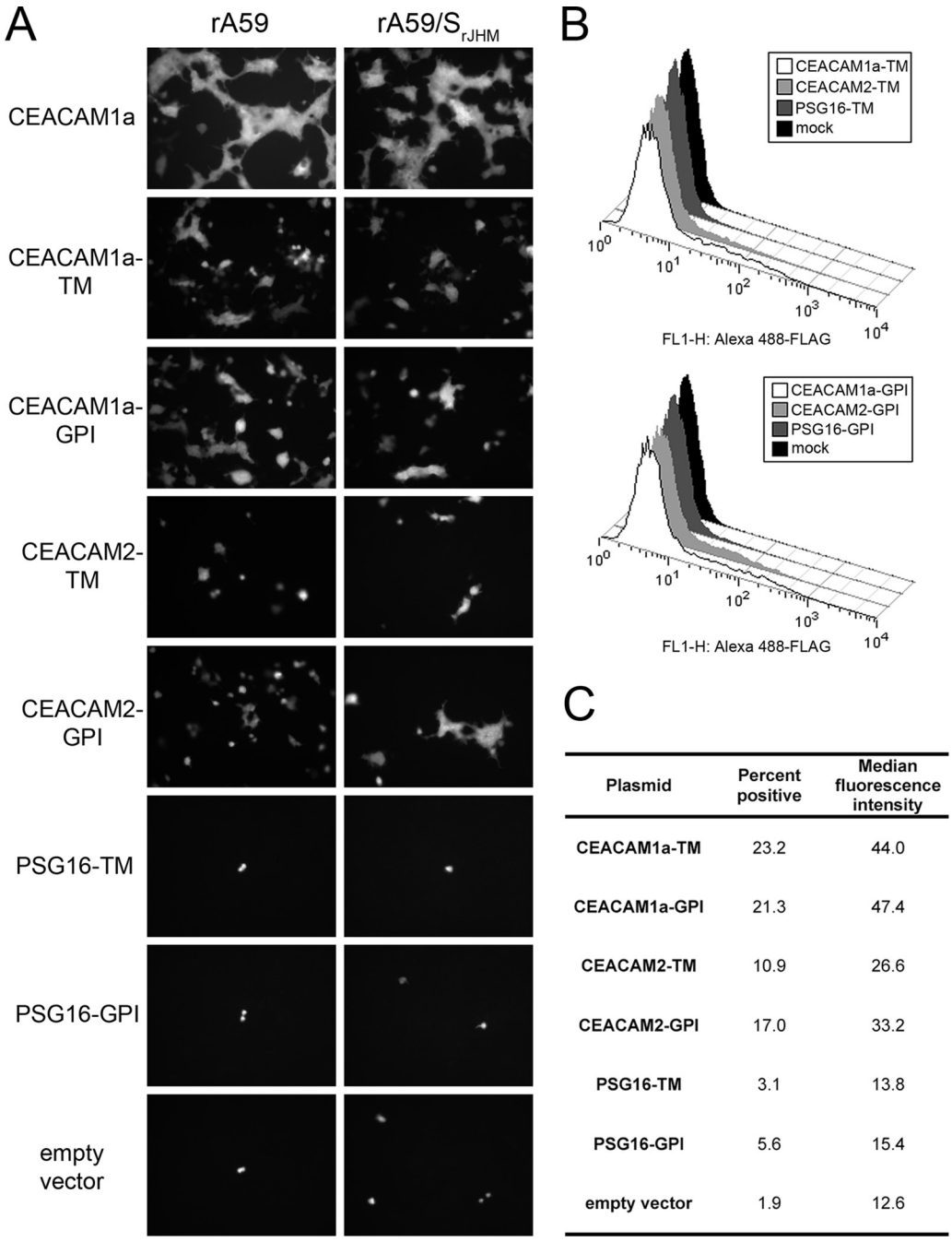


| Plasmid | Percent positive | Median fluorescence intensity |
|---|---|---|
| CEACAM1a-TM | 23.2 | 44.0 |
| CEACAM1a-GPI | 21.3 | 47.4 |
| CEACAM2-TM | 10.9 | 26.6 |
| CEACAM2-GPI | 17.0 | 33.2 |
| PSG16-TM | 3.1 | 13.8 |
| PSG16-GPI | 5.6 | 15.4 |
| empty vector | 1.9 | 12.6 |

FIG. 9. MHV infection and surface expression of TVA-CEA chimeras. Human 293T cells were transfected with expression plasmids encoding CEACAM1a, CEACAM2, and PSG16 extracellular domains with the signal sequence and membrane anchor domains of the avian retrovirus receptor TVA. Plasmids encoding wild-type CEACAM1a and empty vector were transfected as controls. TM, TVA transmembrane anchor; GPI, TVA glycosylphosphatidylinositol anchor. (A) Cells were infected at 48 h posttransfection with approximately 5 PFU/cell of rA59-EGFP or rA59/$S_{JHM.SD}$-EGFP and were fixed at 16 h postinfection for EGFP detection. (B) TVA-CEA-transfected cells were immunolabeled with mouse M2 anti-FLAG antibody and Alexa 488-conjugated goat anti-mouse IgG and were analyzed by flow cytometry. "Mock" represents untransfected 293T cells immunolabeled in parallel. (C) Summary of percent positive cells and median fluorescence intensity for TVA-CEA-transfected cells. Positive cells were defined as those with a fluorescence intensity of >98% that of the mock-transfected cells. Median fluorescence intensity was calculated for the positive population.

the fact that the only CNS cells previously shown to express CEACAM1a are endothelial cells and microglia (17, 44). One possible explanation is that other cell types do express CEACAM1a, but at low levels that are not detectable by routine assays and/or sublocalized (at the neuronal synapse, for example) in such a way that the protein is inaccessible to antibodies. To address these possibilities, we used qRT-PCR to assess the expression of *ceacam1a* mRNA. Overall, our

results support the idea that *ceacam1a* expression alone does not determine MHV cell tropism.

Interpretation of the qRT-PCR results is complicated by several factors. Since we were unable to demonstrate protein expression in the cell cultures studied, it is not at all certain that *ceacam1a* mRNA expression correlates with CEACAM1a protein expression; however, our results for *ceacam1a* mRNA expression in whole-tissue lysates (Fig. 2A) were consistent with published protein data for the liver and brain (17, 59), and *ceacam1a* mRNA expression was highest in the hepatocyte and microglia cell cultures (Fig. 2B), which are known to express CEACAM1a (17, 44), suggesting that the qRT-PCR assay is valid. The low levels of *ceacam1a* expression detected in astrocyte and neuron cultures (Fig. 2B) must be considered with reference to the possibility of microglia contamination. For example, astrocyte cultures were 90 to 95% pure, with microglia being the primary contaminant, but *ceacam1a* expression was 10-fold lower in astrocytes than in microglia, making it difficult to distinguish low-level *ceacam1a* expression in astrocytes from higher-level expression by contaminating microglia. Expression of *ceacam1a* in neuron cultures was similarly compatible with low-level microglia contamination, although the striking difference in neuronal spread observed in WT and *ceacam1a*$^{-/-}$ cultures infected with rA59 (Fig. 5) suggests that WT neurons do express at least some CEACAM1a. The *ceacam1a* expression detected in oligodendrocyte cultures was much less likely to be affected by contamination: the primary contaminant in those cultures was astrocytes, which express lower levels of *ceacam1a* than those detected in the oligodendrocyte cultures, and the inverted ratio of 2D to 4D splice variants (Fig. 3C) was unique to the oligodendrocyte cultures. To reduce the complication of contaminating cells and to investigate *ceacam1a* expression in cells directly *ex vivo*, future studies aim to purify glia from the adult CNS and to isolate RNAs from these purified cell populations as described by Malone et al. (29).

Neurotropic strains of MHV may have evolved a novel mechanism to spread to and between specialized CNS cell types, particularly neurons. Using mixed neural cultures, Nakagaki and Taguchi (34) demonstrated that the highly neurovirulent JHM.SD cl-2 isolate spreads to nonmicroglial cells in the presence of CEACAM1a antibody blockade; in contrast, a soluble receptor-resistant mutant of cl-2, srr7, remains restricted to microglia when CEACAM1a is blocked. From these experiments, it was proposed that initial CNS infection with MHV occurs via entry into CEACAM1a-expressing microglia and that spread to additional CNS cell types requires the capacity for CEACAM1a-independent spread. While microglia may indeed represent an early site of MHV replication in the CNS, this model is insufficient to explain the diverse cellular tropism of rA59 (Fig. 1), particularly since rA59 requires CEACAM1a for spread among adjacent cells *in vitro* (56). Furthermore, while *in vitro* studies indicate that both rA59 and rJHM.SD require CEACAM1a for initial entry (15, 55), this does not seem to be the case *in vivo*, as rJHM.SD can both infect and spread in the CNS of *ceacam1a*$^{-/-}$ mice (33). These results suggest that more than one mechanism may be involved during infection of *ceacam1a*$^{-/-}$ animals, with (i) initial entry in the absence of CEACAM1a and (ii) spread among adjacent cells in the absence of CEACAM1a.

Since MHV entry and spread are difficult to distinguish in the whole brain, we examined MHV entry and spread in an *in vitro* system, using primary neurons, the predominant CNS cell type infected (Fig. 1) (12, 42), in order to separate entry and spread. The ability of all three viruses to enter occasional CEACAM1a KO cells (Fig. 5) was initially surprising, given previous reports that CEACAM1a antibody blockade prevents MHV infection in mixed neural cultures (34). However, given the low incidence of infection seen in *ceacam1a*$^{-/-}$ neurons, it is possible that the phenomenon was not appreciated in these blocking experiments or was attributed to incomplete antibody blockade. Our results suggest that MHV may use a low-efficiency alternative receptor to enter neurons, so we examined the two proposed alternative receptors, CEACAM2 (38) and PSG16 (5), for CNS expression and receptor activity. CEACAM2 does have at least some receptor activity (Fig. 8 and 9). While we would expect CEACAM2 to be a less efficient MHV receptor than CEACAM1a, since the critical MHV spike-binding motif at amino acids 38 to 43 (45) of CEACAM2 is much more similar to the MHV-resistant CEACAM1b allele than to CEACAM1a, the TVA-CEACAM2 chimeras created to analyze surface expression were in fact expressed at lower levels than the TVA-CEACAM1 chimeras (Fig. 9B). Therefore, we cannot exclude the possibility that differences in receptor density and surface distribution also contributed to the lower level of receptor activity observed for CEACAM2. However, the *ceacam2* message was barely detectable in neurons (Fig. 5B) and thus is not likely to play a role in neuronal infection. And while *psg16* (*bCEA*) was expressed well and strikingly specifically in neurons—to our knowledge, this is the first report of a pregnancy-specific glycoprotein family member expressed in cultured neurons—the product failed to support MHV infection (Fig. 8 and 9) or even to reach the cell surface, despite our attempts to target it there with exogenous signal peptide and membrane anchor sequences (Fig. 9). The *psg16* locus does contain an alternative upstream exon 1, encoding a signal sequence and a complete N1 domain homologous to the N domain of CEACAM1a (32). This alternative isoform is predicted to be expressed in the placenta, and if it is expressed in neurons as well, it might have better MHV receptor activity than the published isoform we examined. It is also possible that either PSG16 isoform has neuron-specific receptor activity, for example, if cell surface targeting requires expression in conjunction with another protein or membrane entity that is present in mouse neurons but lacking in 293T cells. In addition, the placental members of the PSG family give low yields in expression systems (Gabriela Dveksler, personal communication), despite demonstrated biological activity (19, 58), so surface levels of PSG16 not detectable by our assay might be sufficient to support MHV infection in neurons. Future experiments are planned to investigate the subcellular localization and MHV receptor activity of the novel PSG16 isoform. At this time, however, neither CEACAM2 nor PSG16 seems to account for MHV entry into *ceacam1a*$^{-/-}$ neurons.

The ability of MHV strains bearing the rJHM.SD spike to spread among *ceacam1a*$^{-/-}$ neurons, while consistent with previous data showing that rJHM.SD but not rA59 successfully infects the CNS of *ceacam1a*$^{-/-}$ mice (33), is puzzling. Widespread infection of neuronal cultures with viruses expressing the rJHM.SD spike appears to occur in the absence of high

levels of infectious virus released, just as previously described for the brain (23, 41). While it should be noted that the JHM.SD spike is inherently less stable than that of A59 and may be inactivated more rapidly following release from an infected cell (14, 24, 53), resulting in an underestimation of the amount of infectious virus produced, this is less likely to be the case for cell-associated virus, for which rJHM.SD titers were also lower than those for rA59 (Fig. 4B). These data suggest that rJHM does in fact spread more efficiently than rA59, even among WT neurons, in which absolute differences in spread are less dramatic (42). One hypothesis is that the rJHM.SD spike is able to use an alternative receptor not available to rA59, but this would require that the receptor in question be localized to regions of close cell membrane juxtaposition, since only spread, not entry, is affected. It is tempting to speculate that spread between *ceacam1a*$^{-/-}$ neurons is related to the JHM.SD-specific phenomenon of RIS, in which cells infected with JHM.SD (15) or expressing the JHM.SD spike (54) fuse with neighboring cells even in the absence of CEACAM1a, allowing viral spread. However, the Iowa strain of JHM (JHM.IA), while not capable of RIS (39), is still highly neurovirulent (28). In addition, it is not clear that spread among adjacent neurons actually involves cell membrane fusion. Future experiments are planned to determine whether receptor-independent spread is in fact responsible for spread among *ceacam1a*$^{-/-}$ neurons. Finally, JHM.SD may have evolved a novel mechanism for axonal trafficking or targeting to the neuronal synapse that enables *trans*-synaptic spread; while we currently have no data to support that hypothesis, such mechanisms have been described for other neurotropic viruses. Whatever the mechanism, it seems likely that the ability of JHM.SD to spread in *ceacam1a*$^{-/-}$ neurons is responsible for the extreme neurovirulence of this strain.

In summary, the less neurovirulent A59 strain of MHV appears to be dependent on the low levels of neuronal CEACAM1a detected in susceptible CNS cells for neuronal spread and CNS disease, while the more virulent JHM.SD strain is able to spread and cause disease even in the absence of CEACAM1a. At this time, it is still uncertain how MHV initially enters or spreads among WT neurons, and we cannot exclude the possibility that a receptor-independent mechanism allows spread from nonneuronal cells to neurons in these cultures. For *ceacam1a*$^{-/-}$ mouse infection, we propose a model in which both rA59 and rJHM.SD can enter occasional CNS cells lacking *ceacam1a* expression; this initial entry may occur via CEACAM2 on endothelial cells, microglia, and/or oligodendrocytes, via an alternative form of PSG16 that has not yet been described or via another, as yet unidentified alternative receptor that can facilitate virus entry, albeit inefficiently. Once initial entry has occurred, a CEACAM1a-independent mechanism allows viruses expressing the JHM.SD spike to spread to adjacent cells and lead to fatal neurological disease, while rA59 remains restricted to individual cells and does not produce detectable CNS infection. This CEACAM1a-independent spread may involve a low-efficiency alternative receptor that mediates spread by rJHM.SD but not by rA59, canonical receptor-independent spread, or a novel mechanism of *trans*-synaptic spread. Future studies using the *ceacam1a*$^{-/-}$ mouse and primary cell models combined with a variety of neurotropic MHV strains differing in tropism and CEACAM1a dependence aim to address the mechanism of CEACAM1a-independent spread in neural cells and the contribution of this process to neurovirulence.

## ACKNOWLEDGMENTS

We thank Jayasri Das Sarma, Marc Dichter, Margaret Maronski, Judith Grinspan, and Mary Reid for assistance with primary cell cultures, Nicole Beauchemin and Kathryn Holmes for *ceacam1a*$^{-/-}$ mice and reagents, and Jessica Roth-Cross and Kristine Rose for helpful advice and discussions.

This work was supported by NIH grant AI-60021 to S.R.W. S.J.B. and E.P.S. were partially supported by NIH training grant NS-07180. J.M.P. was partially supported by NIH training grant AI-07634.

## REFERENCES

1. **Aloisi, F., F. Ria, G. Penna, and L. Adorini.** 1998. Microglia are more efficient than astrocytes in antigen processing and in Th1 but not Th2 cell activation. J. Immunol. **160:**4671–4680.
2. **Banker, G., and K. Goslin (ed.).** 1991. Culturing nerve cells. MIT Press, Cambridge, MA.
3. **Blau, D. M., C. Turbide, M. Tremblay, M. Olson, S. Letourneau, E. Michaliszyn, S. Jothy, K. V. Holmes, and N. Beauchemin.** 2001. Targeted disruption of the Ceacam1 (MHVR) gene leads to reduced susceptibility of mice to mouse hepatitis virus infection. J. Virol. **75:**8173–8186.
4. **Buchmeier, M. J., H. A. Lewicki, P. J. Talbot, and R. L. Knobler.** 1984. Murine hepatitis virus-4 (strain JHM)-induced neurologic disease is modulated in vivo by monoclonal antibody. Virology **132:**261–270.
5. **Chen, D. S., M. Asanaka, K. Yokomori, F. Wang, S. B. Hwang, H. P. Li, and M. M. Lai.** 1995. A pregnancy-specific glycoprotein is expressed in the brain and serves as a receptor for mouse hepatitis virus. Proc. Natl. Acad. Sci. U. S. A. **92:**12095–12099.
6. **Coutelier, J. P., C. Godfraind, G. S. Dveksler, M. Wysocka, C. B. Cardellichio, H. Noel, and K. V. Holmes.** 1994. B lymphocyte and macrophage expression of carcinoembryonic antigen-related adhesion molecules that serve as receptors for murine coronavirus. Eur. J. Immunol. **24:**1383–1390.
7. **Cowley, T. J., S. Y. Long, and S. R. Weiss.** 2010. The murine coronavirus nucleocapsid gene is a determinant of virulence. J. Virol. **84:**1752–1763.
8. **Das Sarma, J., E. Scheen, S. H. Seo, M. Koval, and S. R. Weiss.** 2002. Enhanced green fluorescent protein expression may be used to monitor murine coronavirus spread in vitro and in the mouse central nervous system. J. Neurovirol. **8:**381–391.
9. **Dichter, M. A.** 1978. Rat cortical neurons in cell culture: culture methods, cell morphology, electrophysiology, and synapse formation. Brain Res. **149:** 279–293.
10. **Dveksler, G. S., C. W. Dieffenbach, C. B. Cardellichio, K. McCuaig, M. N. Pensiero, G. S. Jiang, N. Beauchemin, and K. V. Holmes.** 1993. Several members of the mouse carcinoembryonic antigen-related glycoprotein family are functional receptors for the coronavirus mouse hepatitis virus-A59. J. Virol. **67:**1–8.
11. **Dveksler, G. S., M. N. Pensiero, C. W. Dieffenbach, C. B. Cardellichio, A. A. Basile, P. E. Elia, and K. V. Holmes.** 1993. Mouse hepatitis virus strain A59 and blocking antireceptor monoclonal antibody bind to the N-terminal domain of cellular receptor. Proc. Natl. Acad. Sci. U. S. A. **90:**1716–1720.
12. **Fazakerley, J. K., S. E. Parker, F. Bloom, and M. J. Buchmeier.** 1992. The V5A13.1 envelope glycoprotein deletion mutant of mouse hepatitis virus type-4 is neuroattenuated by its reduced rate of spread in the central nervous system. Virology **187:**178–188.
13. **Feigenson, K., M. Reid, J. See, E. B. Crenshaw III, and J. B. Grinspan.** 2009. Wnt signaling is sufficient to perturb oligodendrocyte maturation. Mol. Cell. Neurosci. **42:**255–265.
14. **Gallagher, T. M.** 1997. A role for naturally occurring variation of the murine coronavirus spike protein in stabilizing association with the cellular receptor. J. Virol. **71:**3129–3137.
15. **Gallagher, T. M., M. J. Buchmeier, and S. Perlman.** 1992. Cell receptor-independent infection by a neurotropic murine coronavirus. Virology **191:** 517–522.
16. **Godfraind, C., N. Havaux, K. V. Holmes, and J. P. Coutelier.** 1997. Role of virus receptor-bearing endothelial cells of the blood-brain barrier in preventing the spread of mouse hepatitis virus-A59 into the central nervous system. J. Neurovirol. **3:**428–434.
17. **Godfraind, C., S. G. Langreth, C. B. Cardellichio, R. Knobler, J. P. Coutelier, M. Dubois-Dalcq, and K. V. Holmes.** 1995. Tissue and cellular distribution of an adhesion molecule in the carcinoembryonic antigen family that serves as a receptor for mouse hepatitis virus. Lab. Invest. **73:**615–627.
18. **Gray-Owen, S. D., and R. S. Blumberg.** 2006. CEACAM1: contact-dependent control of immunity. Nat. Rev. Immunol. **6:**433–446.
19. **Ha, C. T., R. Waterhouse, J. Wessells, J. A. Wu, and G. S. Dveksler.** 2005. Binding of pregnancy-specific glycoprotein 17 to CD9 on macrophages in-

duces secretion of IL-10, IL-6, PGE2, and TGF-beta1. J. Leukoc. Biol. **77:**948–957.
20. **Han, E., D. Phan, P. Lo, M. N. Poy, R. Behringer, S. M. Najjar, and S. H. Lin.** 2001. Differences in tissue-specific and embryonic expression of mouse Ceacam1 and Ceacam2 genes. Biochem. J. **355:**417–423.
21. **Hemmila, E., C. Turbide, M. Olson, S. Jothy, K. V. Holmes, and N. Beauchemin.** 2004. Ceacam1a$^{-/-}$ mice are completely resistant to infection by murine coronavirus mouse hepatitis virus A59. J. Virol. **78:**10156–10165.
22. **Hirano, N., K. Fujiwara, S. Hino, and M. Matumoto.** 1974. Replication and plaque formation of mouse hepatitis virus (MHV-2) in mouse cell line DBT culture. Arch. Gesamte Virusforsch. **44:**298–302.
23. **Iacono, K. T., L. Kazi, and S. R. Weiss.** 2006. Both spike and background genes contribute to murine coronavirus neurovirulence. J. Virol. **80:**6834–6843.
24. **Krueger, D. K., S. M. Kelly, D. N. Lewicki, R. Ruffolo, and T. M. Gallagher.** 2001. Variations in disparate regions of the murine coronavirus spike protein impact the initiation of membrane fusion. J. Virol. **75:**2792–2802.
25. **Kuespert, K., S. Pils, and C. R. Hauck.** 2006. CEACAMs: their role in physiology and pathophysiology. Curr. Opin. Cell Biol. **18:**565–571.
26. **Lavi, E., D. H. Gilden, M. K. Highkin, and S. R. Weiss.** 1986. The organ tropism of mouse hepatitis virus A59 in mice is dependent on dose and route of inoculation. Lab. Anim. Sci. **36:**130–135.
27. **MacNamara, K. C., S. J. Bender, M. M. Chua, R. Watson, and S. R. Weiss.** 2008. Priming of CD8$^+$ T cells during central nervous system infection with a murine coronavirus is strain dependent. J. Virol. **82:**6150–6160.
28. **MacNamara, K. C., M. M. Chua, J. J. Phillips, and S. R. Weiss.** 2005. Contributions of the viral genetic background and a single amino acid substitution in an immunodominant CD8$^+$ T-cell epitope to murine coronavirus neurovirulence. J. Virol. **79:**9108–9118.
29. **Malone, K. E., S. A. Stohlman, C. Ramakrishna, W. Macklin, and C. C. Bergmann.** 2008. Induction of class I antigen processing components in oligodendroglia and microglia during viral encephalomyelitis. Glia **56:**426–435.
30. **McCuaig, K., M. Rosenberg, P. Nedellec, C. Turbide, and N. Beauchemin.** 1993. Expression of the Bgp gene and characterization of mouse colon biliary glycoprotein isoforms. Gene **127:**173–183.
31. **McCuaig, K., C. Turbide, and N. Beauchemin.** 1992. mmCGM1a: a mouse carcinoembryonic antigen gene family member, generated by alternative splicing, functions as an adhesion molecule. Cell Growth Differ. **3:**165–174.
32. **McLellan, A. S., B. Fischer, G. Dveksler, T. Hori, F. Wynne, M. Ball, K. Okumura, T. Moore, and W. Zimmermann.** 2005. Structure and evolution of the mouse pregnancy-specific glycoprotein (Psg) gene locus. BMC Genomics **6:**4.
33. **Miura, T. A., E. A. Travanty, L. Oko, H. Bielefeldt-Ohmann, S. R. Weiss, N. Beauchemin, and K. V. Holmes.** 2008. The spike glycoprotein of murine coronavirus MHV-JHM mediates receptor-independent infection and spread in the central nervous systems of Ceacam1a$^{-/-}$ mice. J. Virol. **82:**755–763.
34. **Nakagaki, K., and F. Taguchi.** 2005. Receptor-independent spread of a highly neurotropic murine coronavirus JHMV strain from initially infected microglial cells in mixed neural cultures. J. Virol. **79:**6102–6110.
35. **Nakajima, A., H. Iijima, M. F. Neurath, T. Nagaishi, E. E. Nieuwenhuis, R. Raychowdhury, J. Glickman, D. M. Blau, S. Russell, K. V. Holmes, and R. S. Blumberg.** 2002. Activation-induced expression of carcinoembryonic antigen-cell adhesion molecule 1 regulates mouse T lymphocyte function. J. Immunol. **168:**1028–1035.
36. **Nash, T. C., and M. J. Buchmeier.** 1996. Spike glycoprotein-mediated fusion in biliary glycoprotein-independent cell-associated spread of mouse hepatitis virus infection. Virology **223:**68–78.
37. **Navas, S., and S. R. Weiss.** 2003. Murine coronavirus-induced hepatitis: JHM genetic background eliminates A59 spike-determined hepatotropism. J. Virol. **77:**4972–4978.
38. **Nedellec, P., G. S. Dveksler, E. Daniels, C. Turbide, B. Chow, A. A. Basile, K. V. Holmes, and N. Beauchemin.** 1994. Bgp2, a new member of the carcinoembryonic antigen-related gene family, encodes an alternative receptor for mouse hepatitis viruses. J. Virol. **68:**4525–4537.
39. **Ontiveros, E., T. S. Kim, T. M. Gallagher, and S. Perlman.** 2003. Enhanced virulence mediated by the murine coronavirus, mouse hepatitis virus strain JHM, is associated with a glycine at residue 310 of the spike glycoprotein. J. Virol. **77:**10260–10269.
40. **Pasick, J. M., K. Kalicharran, and S. Dales.** 1994. Distribution and trafficking of JHM coronavirus structural proteins and virions in primary neurons and the OBL-21 neuronal cell line. J. Virol. **68:**2915–2928.
41. **Phillips, J. J., M. M. Chua, E. Lavi, and S. R. Weiss.** 1999. Pathogenesis of chimeric MHV4/MHV-A59 recombinant viruses: the murine coronavirus spike protein is a major determinant of neurovirulence. J. Virol. **73:**7752–7760.
42. **Phillips, J. J., M. M. Chua, G. F. Rall, and S. R. Weiss.** 2002. Murine coronavirus spike glycoprotein mediates degree of viral spread, inflammation, and virus-induced immunopathology in the central nervous system. Virology **301:**109–120.
43. **Rall, G. F., L. Mucke, and M. B. Oldstone.** 1995. Consequences of cytotoxic T lymphocyte interaction with major histocompatibility complex class I-expressing neurons in vivo. J. Exp. Med. **182:**1201–1212.
44. **Ramakrishna, C., C. C. Bergmann, K. V. Holmes, and S. A. Stohlman.** 2004. Expression of the mouse hepatitis virus receptor by central nervous system microglia. J. Virol. **78:**7828–7832.
45. **Rao, P. V., S. Kumari, and T. M. Gallagher.** 1997. Identification of a contiguous 6-residue determinant in the MHV receptor that controls the level of virion binding to cells. Virology **229:**336–348.
46. **Rong, L., and P. Bates.** 1995. Analysis of the subgroup A avian sarcoma and leukosis virus receptor: the 40-residue, cysteine-rich, low-density lipoprotein receptor repeat motif of Tva is sufficient to mediate viral entry. J. Virol. **69:**4847–4853.
47. **Rong, L., K. Gendron, and P. Bates.** 1998. Conversion of a human low-density lipoprotein receptor ligand binding repeat to a virus receptor: identification of residues important for ligand specificity. Proc. Natl. Acad. Sci. U. S. A. **95:**8467–8472.
48. **Roth-Cross, J. K., S. J. Bender, and S. R. Weiss.** 2008. Murine coronavirus mouse hepatitis virus is recognized by MDA5 and induces type I interferon in brain macrophages/microglia. J. Virol. **82:**9829–9838.
49. **Roth-Cross, J. K., L. Martinez-Sobrido, E. P. Scott, A. Garcia-Sastre, and S. R. Weiss.** 2007. Inhibition of the IFN-alpha/beta response by mouse hepatitis virus (MHV) at multiple levels. J. Virol. **81:**7189–7199.
50. **Snodgrass, S. R., W. F. White, B. Biales, and M. Dichter.** 1980. Biochemical correlates of GABA function in rat cortical neurons in culture. Brain Res. **190:**123–138.
51. **Strausberg, R. L., E. A. Feingold, L. H. Grouse, J. G. Derge, R. D. Klausner, F. S. Collins, L. Wagner, C. M. Shenmen, G. D. Schuler, S. F. Altschul, B. Zeeberg, K. H. Buetow, C. F. Schaefer, N. K. Bhat, R. F. Hopkins, H. Jordan, T. Moore, S. I. Max, J. Wang, F. Hsieh, L. Diatchenko, K. Marusina, A. A. Farmer, G. M. Rubin, L. Hong, M. Stapleton, M. B. Soares, M. F. Bonaldo, T. L. Casavant, T. E. Scheetz, M. J. Brownstein, T. B. Usdin, S. Toshiyuki, P. Carninci, C. Prange, S. S. Raha, N. A. Loquellano, G. J. Peters, R. D. Abramson, S. J. Mullahy, S. A. Bosak, P. J. McEwan, K. J. McKernan, J. A. Malek, P. H. Gunaratne, S. Richards, K. C. Worley, S. Hale, A. M. Garcia, L. J. Gay, S. W. Hulyk, D. K. Villalon, D. M. Muzny, E. J. Sodergren, X. Lu, R. A. Gibbs, J. Fahey, E. Helton, M. Ketteman, A. Madan, S. Rodrigues, A. Sanchez, M. Whiting, A. C. Young, Y. Shevchenko, G. G. Bouffard, R. W. Blakesley, J. W. Touchman, E. D. Green, M. C. Dickson, A. C. Rodriguez, J. Grimwood, J. Schmutz, R. M. Myers, Y. S. Butterfield, M. I. Krzywinski, U. Skalska, D. E. Smailus, A. Schnerch, J. E. Schein, S. J. Jones, and M. A. Marra.** 2002. Generation and initial analysis of more than 15,000 full-length human and mouse cDNA sequences. Proc. Natl. Acad. Sci. U. S. A. **99:**16899–16903.
52. **Sturman, L. S., K. V. Holmes, and J. Behnke.** 1980. Isolation of coronavirus envelope glycoproteins and interaction with the viral nucleocapsid. J. Virol. **33:**449–462.
53. **Sturman, L. S., C. S. Ricard, and K. V. Holmes.** 1990. Conformational change of the coronavirus peplomer glycoprotein at pH 8.0 and 37 degrees C correlates with virus aggregation and virus-induced cell fusion. J. Virol. **64:**3042–3050.
54. **Taguchi, F., T. Ikeda, and H. Shida.** 1992. Molecular cloning and expression of a spike protein of neurovirulent murine coronavirus JHMV variant cl-2. J. Gen. Virol. **73:**1065–1072.
55. **Taguchi, F., S. Matsuyama, and K. Saeki.** 1999. Difference in Bgp-independent fusion activity among mouse hepatitis viruses. Arch. Virol. **144:**2041–2049.
56. **Tsai, J. C., B. D. Zelus, K. V. Holmes, and S. R. Weiss.** 2003. The N-terminal domain of the murine coronavirus spike glycoprotein determines the CEACAM1 receptor specificity of the virus strain. J. Virol. **77:**841–850.
57. **Weiss, S. R., and S. Navas-Martin.** 2005. Coronavirus pathogenesis and the emerging pathogen severe acute respiratory syndrome coronavirus. Microbiol. Mol. Biol. Rev. **69:**635–664.
58. **Wessells, J., D. Wessner, R. Parsells, K. White, D. Finkenzeller, W. Zimmermann, and G. Dveksler.** 2000. Pregnancy specific glycoprotein 18 induces IL-10 expression in murine macrophages. Eur. J. Immunol. **30:**1830–1840.
59. **Williams, R. K., G. S. Jiang, and K. V. Holmes.** 1991. Receptor for mouse hepatitis virus is a member of the carcinoembryonic antigen family of glycoproteins. Proc. Natl. Acad. Sci. U. S. A. **88:**5533–5536.